Supporting Information

Ternary-Phase Nanostructure W_3P/WP/W for High-Performance pH-Universal Water/Seawater Electrolysis

Dongkui Huo, Zhichao Sun*, Yingya Liu, Zhiquan Yu, Yao Wang*, Anjie Wang

State Key Laboratory of Fine Chemicals, and Liaoning Key Laboratory of Petrochemical Technology and Equipments, Dalian University of Technology, Dalian 116024, PR China

*Corresponding author:
Yao Wang: wangyao@dlut.edu.cn
Zhichao Sun: sunzhichao@dlut.edu.cn

Number of pages: 38
Number of figures: 24
Number of tables: 11

1. Experimental section

1.1 Materials

Ammonium metatungstate hydrate ($(NH_4)_6W_{12}O_{39}\cdot xH_2O$) and citric acid (CA) were purchased from Macklin. Ammonium phosphate dibasic ($(NH_4)_2HPO_4$) was obtained from Sinopharm Chemical Reagent Co., Ltd. Besides, commercial Pt/C (20 wt%) and 5 wt% Nafion solution were acquired from Sigma-Aldrich and DuPont Company (USA), respectively. All these chemicals were of analytical grade and can be directly used without further purification. Furthermore, ion exchange resin (A861683 from Macklin) needs extra pretreatments before use and regeneration to be reused (details are shown in Supporting Information: ion exchange resin purified seawater part). All the solutions were prepared by deionized water unless otherwise specified.

1.2 Electrocatalysts Synthesis

1.2.1 W_3P/WP/W:

Firstly, $(NH_4)_6W_{12}O_{39}\cdot xH_2O$, $(NH_4)_2HPO_4$, and citric acid were as-weighed and dissolved by deionized water respectively at a mole ratio of (W: P: CA=3:1:2). Then, the two solutions containing citric acid and $(NH_4)_6W_{12}O_{39}\cdot xH_2O$ were mixed, followed by magnetic stirring for 12 hours at a temperature of 90 ℃. Next, the $(NH_4)_2HPO_4$ solution was added into the as-treated solution drop by drop, and simultaneously, the temperature was set to 120 ℃ for the purpose of removing moisture. After that, the solid sample was sent into a drying oven for overnight drying. Then, the sample was placed into a crucible for calcination of 3 hours at 500 ℃. Until now, the precursor has been successfully synthesized. To get the final electrocatalysts, a TPR process is essential. The programming goes like this: The temperature rises from room temperature to 400 ℃ at a rate of 2 ℃/min and maintains for 10 minutes. After that, a slower heating rate (1 ℃/min) is adopted until the final temperature X (X= 700, 750, 800, 850, 900 ℃). All the as-stated programming is operated in the atmosphere of H_2 (150 $mL\cdot min^{-1}$). Afterward, the samples were naturally cooled down to room temperature. Finally, after passivation in O_2/Ar (0.5 vol%) flow, the catalysts were collected, grounded, and denoted as TPM-1 (750 ℃), TPM-2 (800 ℃), TPM-3 (850 ℃), TPM-4 (900 ℃).
If we only change the initial mole ratio of W: P: CA to 1:1:2, the final temperature to 850 ℃, while other procedures are the same, we will get the sample, WP.

1.2.2 WP/W, W_3P/WP:

We set the initial molar ratio to (W: P: CA=1:1:2) and synthesized the precursor from this. Then the precursor and $(NH_4)_6W_{12}O_{39}\cdot xH_2O$ are thoroughly mixed and calcined

in equimolar, and finally with the same TPR program, and the obtained product is WP/W.

To obtain W_3P/WP, the annealed nanoparticles (TPM-3) were etched in concentrated hydrochloric acid (36.5 wt%) with stirring and heating for over 24 hours (***Caution***! Pay attention to the volatilization of concentrated hydrochloric acid). The resultants were collected by high-speed centrifugation, washed, and then vacuum-dried.

1.2.3 Pure tungsten powder (W):

A certain amount of $(NH_4)_6W_{12}O_{39}\cdot xH_2O$ was calcinated for 3 hours in a muffle furnace at 500 ℃. Then, the powder was reduced at 850 ℃ in a hydrogen flow to get the pure tungsten powder (W).

1.3 Preparation of working electrodes

Typically, we obtained an ink slurry containing electrocatalyst (5 mg), ultrapure water (20 μL), and absolute ethanol (980 μL) by an ultrasonic dispersing for approximately 30 minutes. Then, 50 μL Nafion solution was added into the ink followed by another 30 min sonicating to ensure the homogeneousness. Subsequently, 5 μL of ink was carefully dropped onto a pre-polished glassy carbon electrode (GCE, 5 mm in diameter) with the assistance of a pipette and naturally dried at room temperature. The loading of the working electrode is about 121.5 μg cm^{-2}.

1.4 Materials Characterization

X-ray powder diffraction was adopted to elucidate the phase composition of the catalysts (Rigaku D2400, Japan, using Cu-Kα radiation). For a further investigation on the morphology and microstructure, three efficient approaches were used: field emission scanning electron microscopy (SEM, JSM-7610F Plus, Japan), transmission electron microscopy (TEM, JEM F200, Japan), and high-resolution TEM (HRTEM, JEM F200, Japan). Furthermore, the Energy Dispersive Spectrometer (EDS) spectroscopes attached to the TEM can vividly depict the elemental surface distribution. An inductively coupled plasma optical emission spectroscopy (ICP-OES, AVIO 500, Japan) will provide more detailed data for bulk elemental analysis. Besides, we employed X-ray photoelectron spectroscopy (XPS, Thermo Escalab 250, Thermo Fisher Scientific Ltd., UK) to unveil the chemical state of the elements. All the XPS results were calibrated by the binding energy of the C 1s line (284.8 eV). The BET specific surface area was clarified by the N_2 adsorption/desorption isotherms using Micromeritics Tristar II 3020 (USA) after an overnight vacuum drying.

1.5 Evaluation of Electrocatalytic Activity

All electrocatalytic activity tests are carried out at 25 ℃ through a standard three-electrode system on the CHI 650E workstation (China CH Instruments). We chose platinum plate and modified glassy carbon electrodes (GCE) as the counter and working electrodes. And Ag/AgCl electrode (acid and neutral electrolyte), Hg/HgO (alkaline electrolyte, and seawater-related electrolytes) are used as reference electrodes. Different environments of pH are realized by 0.5 M H_2SO_4 (pH=0) for acid one, 1 M KOH (pH=14.0) for alkaline one, 1 M phosphate-buffered saline (PBS, pH=7.1) for a neutral testing condition. Besides, the simulated seawater contains 1 M KOH, 0.5 M NaCl, 41.2 mM $MgCl_2$ and 12.5 mM $CaCl_2$. More details of the natural seawater are available in the electrochemical evaluation part. To eliminate the impact of dissolved oxygen, nitrogen was inlet before all the tests. In all measurements, the electrochemical potential is converted to a reversible hydrogen electrode (V vs. RHE) by the following formula:

$$E(RHE) = E(reference\ electrode) + 0.197\ + 0.059 \times pH \quad (1)$$

To ensure the working electrode is in stable working condition, we usually conduct a cyclic voltammetry (CV) test of 100 cycles to activate the working electrode before all the electrochemical experiments. The sweep rate of linear sweep voltammetry (LSV) is 2 mV s^{-1}. The results were revised by ohmic potential drop (iR) compensation and changed into their absolute value form. After taking CV measurements for 1000 cycles, an LSV test was conducted to detect the long-term cycling stability. And at the potential corresponding to a current density of 10 or 100 mA cm^{-2}, the current-time tests were conducted. Electrochemical impedance spectroscopy (EIS) data were obtained on the parameters: 10^5 Hz to 0.1 Hz in frequency range and a sinusoidal amplitude of 5 mV. All the EIS data and current densities were calibrated to the geometric surface area of the working electrode.

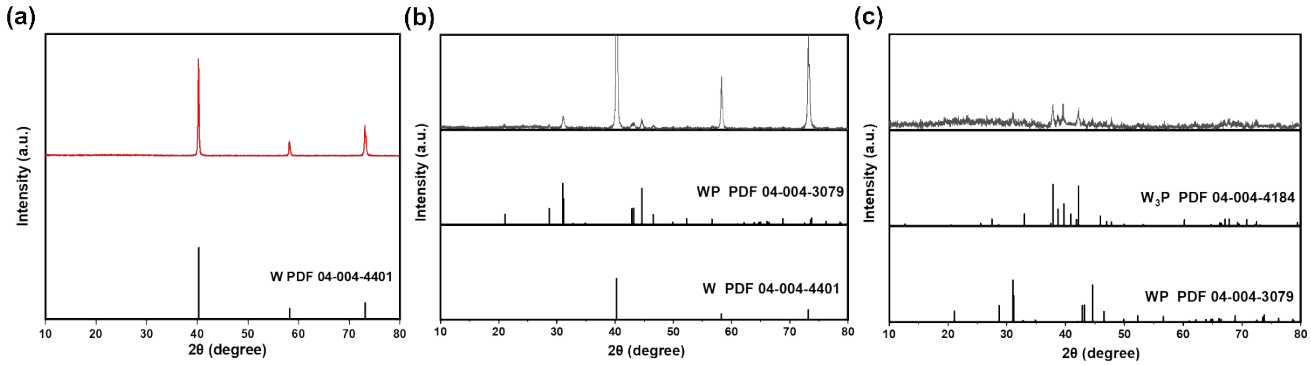

Figure S1. XRD patterns of power W (a), WP/W (b), and W_3P/WP (c).

Table S1a. Physicochemical properties of the catalysts.

Catalyst	Bulk W/P [1)]	Surface W/P [2)]	Phase mole ratio W_3P:WP:W [3)]	Phase mole ratio (W_3P+WP)/W [3)]	Calculated Bulk W/P [3)]
TPM-1	4.53	1.79	0.206:0.068:0.726	0.377	5.15
TPM-2	3.45	1.56	0.224:0.173:0.603	0.658	3.65
TPM-3	3.16	1.02	0.277:0.124:0.599	0.669	3.38
TPM-4	5.49	2.96	0.185:0.050:0.765	0.307	5.83

Table S1b. Physicochemical properties of the catalysts.

Catalyst	Crystal size (nm) [4)]	Particle size (nm) [5)]	Crystallinity (%) [4)]	S_{BET} ($m^2 \cdot g^{-1}$) [6)]
TPM-1	58.7±13.4	46.9	71.1	11.8
TPM-2	45.8±7.6	38.7	85.3	6.8
TPM-3	26.4±6.6	21.2	92.9	4.6
TPM-4	80.4±14.9	70.2	90.2	1.2

Determined by: 1) ICP; 2) XPS; 3) Jade and PDF-4 +2009; 4) Scherrer equation; 5) TEM; 6) N_2 adsorption/desorption isotherms.

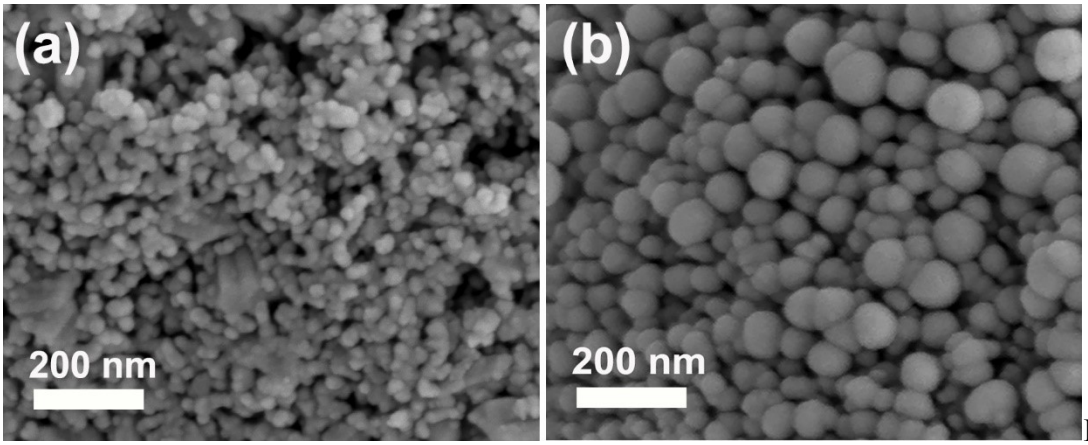

Figure S2. Particle radius increases from TPM-3 to TPM-4, indicating an overgrowth at a higher temperature**.** SEM image of TPM-3 (a) and TPM-4 (b).

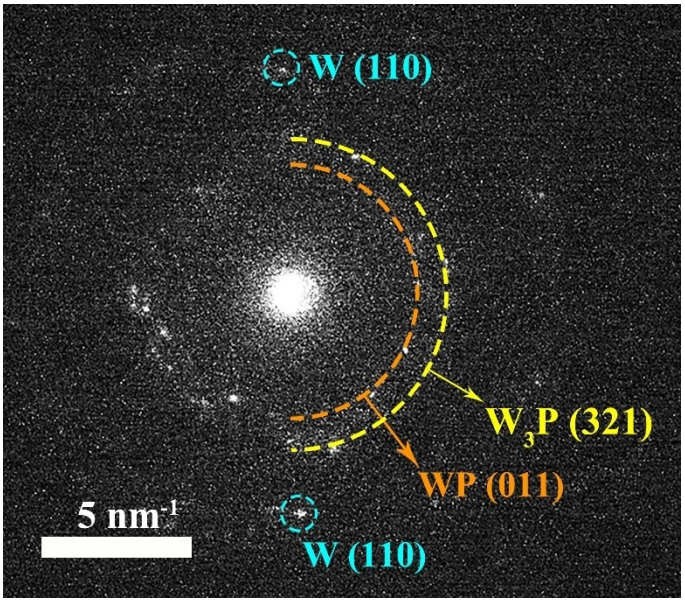

Figure S3. SAED pattern of TPM-3

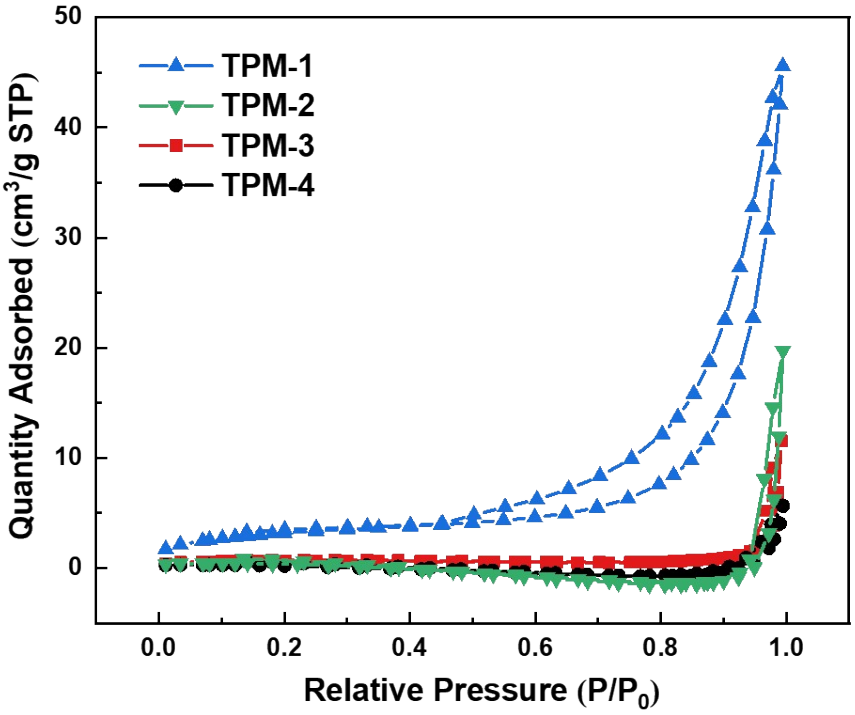

Figure S4. N_2 adsorption-desorption isotherms of the TPMs.

Table S2. Summary of representative WP-based HER catalysts in 0.5 M H_2SO_4.

Catalysts	η_{10} (mV)	Tafel slope	Loading (mg cm^{-2})	Journal
W_2C/WP@NC-2[1]	196	77	1	ACS applied materials & interfaces (2021)
$Co_{0.9}W_{1.1}P_2/C$[2]	35	34	0.283	Nano Research (2021)
CoWP-CA/KB[3]	111	58	0.1215	ACS Sustainable Chemistry & Engineering (2021)
a-WNP[4]	70	39	1	J. Mater. Chem. A (2021)
WP_2 NS/CC[5]	175	103	0.6	International Journal of Hydrogen Energy (2020)
WP-Mesop[6]	104	58	2	ACS applied materials & interfaces (2020)
WP Nano[6]	187	76	2	ACS applied materials & interfaces (2020)
WP@WS_2/C[7]	115	98	2	Chem. ElectroChem (2020)
CoWP[8]	139	65	0.2	Applied Catalysis B: Environmental (2019)
W-SAC[9]	105	58	0.204	Advanced Materials (2018)
WP@CFs[10]	137	69	1	Applied Surface Science(2018)
W_2C/WP@NC[11]	83	61	0.64	Electrochmica Acta (2018)
C-WP/W[12]	109	67	5	Chem. Eng. J, 327 (2017)
Bulk WP[13]	306	78	1.98	J. Mater. Chem. A (2016)
WP@NC[13]	102	58	1.98	J. Mater. Chem. A (2016)
W-Mo-P/CC[14]	93	52	0.213	Energy Environ. Sci. (2016)
W_3P/WP/W	**94**	**58**	**0.1215**	**This work**

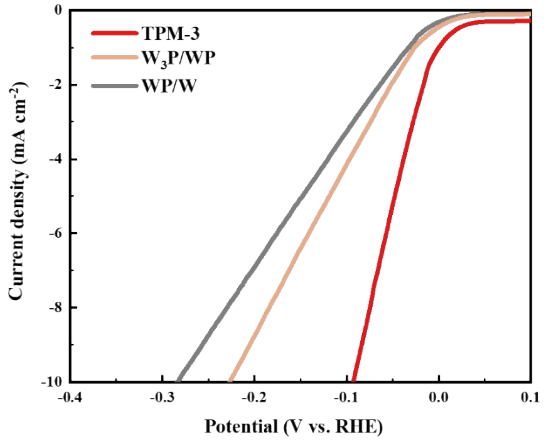

Figure S5. LSV curves of TMP-3, W_3P/WP, and WP/W in 0.5 M H_2SO_4.

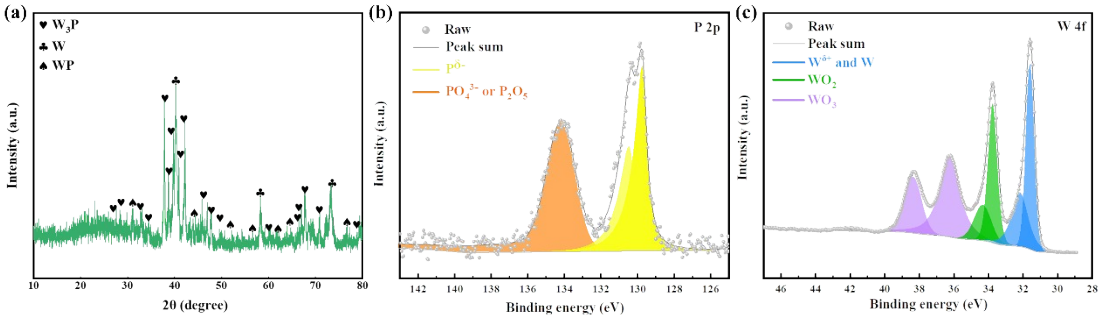

Figure S6. Characterizations of the catalyst after long-term stability test in 0.5 M H_2SO_4. (a) XRD pattern; (b) XPS P 2p; (c) XPS W 4f.

Table S3. Electrochemical impedance parameters obtained by fitting the Nyquist Plots to the equivalent circuit model (0.5 M H_2SO_4)

Catalyst	R_s (Ω)	R_p (Ω)	R_{ct} (Ω)
TPM-1	65.05	18.21	20.47
TPM-2	48.82	16.31	17.83
TPM-3	53.90	23.02	7.406
TPM-4	56.31	30.18	28.53
W_3P/WP	63.24	87.97	35.66
WP/W	58.92	35.41	64.38

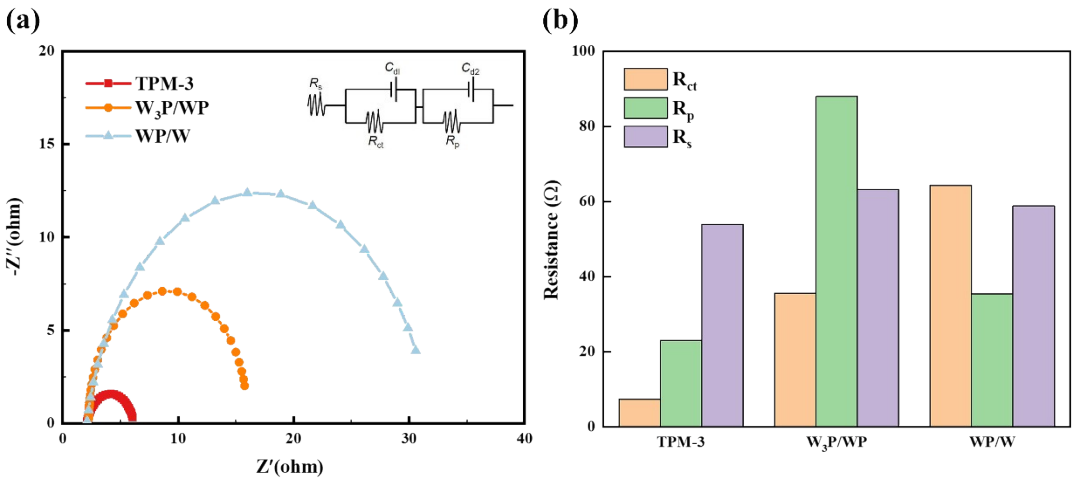

Figure S7. Fitted Nyquist plots of TPM-3, W_3P/WP, and WP/W (a), and their R_{ct}, R_p, and R_s in 0.5 M H_2SO_4 (b). R_s - series resistance, R_{ct} - surface-charge resistance for HER, R_p - resistance related to the surface porosity and conductivity.

Electrochemically Active Surface Area

The electrochemical capacitance measurements were conducted by cyclic voltammograms with various scan rates (20, 40, 60, 80, 100, 120, 140 mV s^{-1}) in 0.5 M H_2SO_4 (0.1~0.45 V), 1 M KOH (0~0.4 V), 1 M PBS (0~0.4 V), respectively. The capacitive currents were measured in a potential range where no faradic processes were observed, i.e., at 0.34 V vs. RHE for 0.5 M H_2SO_4 (Figure. S7), at 0.23V vs. RHE for 1 M KOH (Fig. S12), at 0.20V vs. RHE for 1 M PBS (Fig. S14).

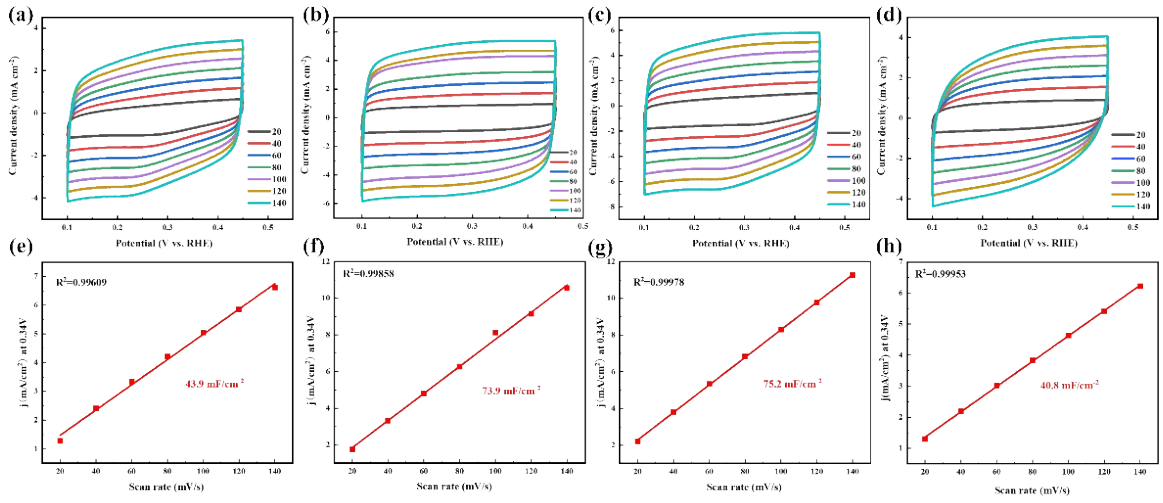

Figure S8. Cyclic voltammograms (a, b, c, d) and their corresponding plots (e, f, g, h) of the current density vs scan rate: TPM-1 (a, e), TPM-2 (b, f), TPM-3 (c, g), and TPM-4 (d, h) in 0.5 M H_2SO_4

According to the previous report[15], the specific capacitance, a flat standard with1 cm^2 of real surface area, is approximately 40 μF cm^{-2}. Thus, the electrochemically active surface area can be calculated by the following formula:

$$A_{ECSA} = \frac{\text{electrochemical capacitance}}{40\ \mu F\ cm^{-2}\ \text{per}\ cm^2_{ECSA}} \quad (1)$$

Calculated Electrochemically Active Surface Area

For 0.5 M H_2SO_4,

TPM-1:

$$\text{ATPM-1 ECSA} = \frac{43.9/2\ mF\ cm^{-2}}{40\ \mu F\ cm^{-2}\ \text{per}\ cm^2_{ECSA}} = 548.75\ \text{cm2 ECSA}$$

TPM-2:

$$\text{ATPM-2 ECSA} = \frac{73.9/2\ mF\ cm^{-2}}{40\ \mu F\ cm^{-2}\ \text{per}\ cm^2_{ECSA}} = 923.75\ \text{cm2 ECSA}$$

TPM-3:

$$\text{ATPM-3 ECSA} = \frac{75.2/2\ mF\ cm^{-2}}{40\ \mu F\ cm^{-2}\ \text{per}\ cm^2_{ECSA}} = 940.00\ \text{cm2 ECSA}$$

TPM-4:

$$\text{ATPM-4 ECSA} = \frac{40.8/2\ mF\ cm^{-2}}{40\ \mu F\ cm^{-2}\ \text{per}\ cm^2_{ECSA}} = 510.00\text{cm2 ECSA}$$

Turnover Frequency Calculations

The turnover frequency can be calculated by the following formula:

$$\text{TOF} = \frac{\text{no. of total hydrogen turnovers/ cm}^2\text{ of geometric area}}{\text{no. of active sites/ cm}^2\text{ of geometric area}}$$

The total number of hydrogen turnovers per current density can be calculated by the formula:

$$\text{No. of } H_2 \text{ (per } \frac{\text{mA}}{\text{cm}^2}\text{)} = \left(\frac{1\text{ C s}^{-1}}{1000\text{ mA}}\right)\left(\frac{1\text{ mol of e}}{96485.3\text{ C}}\right)\left(\frac{1\text{ mol of } H_2}{2\text{ mol of e}}\right)\left(\frac{6.022 \times 10^{23} H_2\text{ molecules}}{1\text{ mol of } H_2}\right)$$

$$= 3.12\times10^{15} \frac{\frac{H_2\text{ s}^{-1}}{\text{cm}^2}}{\text{per } \frac{\text{mA}}{\text{cm}^2}}$$

Active sites per real surface area:

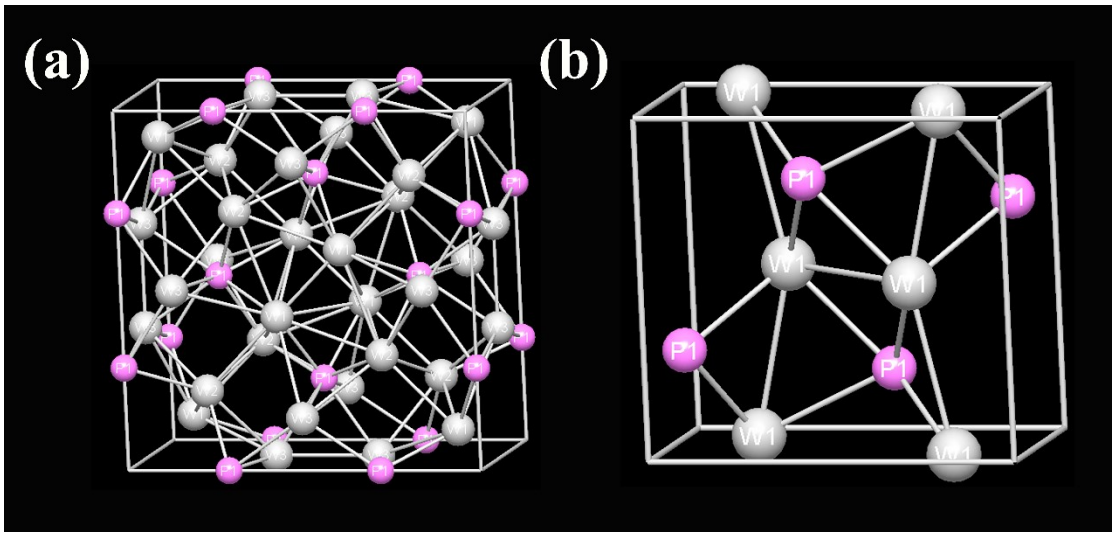

Figure S9. Crystal structure of W_3P (a) and WP (b), W atoms: gray; P atoms: purple.

Table S4. Cell parameters of W_3P and WP.

Crystal	Space group	a (Å)	b (Å)	c (Å)	V (Å^3)
W_3P	I-42m (121)	9.858	9.858	4.800	466.46
WP	Pbnm (62)	6.219	5.717	3.238	115.91

First, let's calculate the active sites. Because TPMs have different compositions, we need to calculate the value of each TPM separately. As demonstrated, the active phases are mainly W_3P and WP, and their molar ratios are given in Table S1a. After normalization, the proportions (W_3P: WP) in each TPM are: TPM-1 (0.752:0.248), TPM-2 (0.564:0.436), TPM-3 (0.691, 0.306), TPM-4 (0.787:0.213).

Active sites of WP= $\left(\frac{8\ \text{atoms/ unit cell}}{115.91\text{Å}^3\text{/ unit cell}}\right)^{\frac{2}{3}} \times 10^{16} = 1.6826\times10^{15}$ atoms cm-2 real

Active sites of W_3P= $\left(\frac{32 \text{ atoms/ unit cell}}{466.46\text{Å}^3/\text{ unit cell}}\right)^{\frac{2}{3}} \times 10^{16} = 1.6758 \times 10^{15}$ atoms cm-2 real

Thus, active sites of

TPM-1: $(0.752 \times 1.6826 + 0.248 \times 1.6758) \times 10^{16} = 1.6809 \times 10^{15}$ atoms cm-2 real

TPM-2: $(0.564 \times 1.6826 + 0.436 \times 1.6758) \times 10^{16} = 1.6796 \times 10^{15}$ atoms cm-2 real

TPM-3: $(0.691 \times 1.6826 + 0.306 \times 1.6758) \times 10^{16} = 1.6755 \times 10^{15}$ atoms cm-2 real

TPM-4: $(0.787 \times 1.6826 + 0.213 \times 1.6758) \times 10^{16} = 1.6812 \times 10^{15}$ atoms cm-2 real

Finally, the plot of current density can be converted into a TOF plot according to:

$$\text{TOF} = \frac{\left(3.12 \times 10^{15} \frac{\text{H}_2\ \text{s}^{-1}}{\text{cm}^2} \text{ per } \frac{\text{mA}}{\text{cm}^2}\right) \times |\text{j}|}{(Active\ sites) \times A_{ECSA}}$$

Then calculate TOF values at an overpotential of -300 mV.

TPM-1:

$$\text{TOF}_{\text{TPM-1}} = \frac{\left(3.12 \times 10^{15} \frac{\text{H}_2\ \text{s}^{-1}}{\text{cm}^2} \text{ per } \frac{\text{mA}}{\text{cm}^2}\right) \times \left| -20.10\text{mA cm}^{-2} \right|}{\left(1.6809 \times 10^{15} \text{ atoms cm}_{\text{real}}^{-2}\right) \times 548.75 \text{ cm}_{\text{ECSA}}^{2}} = 0.068\ \text{H}_2\ \text{s}^{-1}$$

TPM-2:

$$TOF_{TPM\text{-}2} = \frac{(3.12 \times 10^{15} \frac{H_2\ s^{-1}}{cm^2}\ per\ \frac{mA}{cm^2}) \times |-26.72\ mA\ cm^{-2}|}{(1.6796 \times 10^{15}\ atoms\ cm_{real}^{-2}) \times 923.75\ cm_{ECSA}^{2}} = 0.054\ H_2\ s^{-1}$$

TPM-3:

$$TOF_{TPM\text{-}3} = \frac{(3.12 \times 10^{15} \frac{H_2\ s^{-1}}{cm^2}\ per\ \frac{mA}{cm^2}) \times |-33.41\ mA\ cm^{-2}|}{(1.6755 \times 10^{15}\ atoms\ cm_{real}^{-2}) \times 940\ cm_{ECSA}^{2}} = 0.066\ H_2\ s^{-1}$$

TPM-4:

$$TOF_{TPM\text{-}4} = \frac{(3.12 \times 10^{15} \frac{H_2\ s^{-1}}{cm^2}\ per\ \frac{mA}{cm^2}) \times |-15.37\ mA\ cm^{-2}|}{(1.6812 \times 10^{15}\ atoms\ cm_{real}^{-2}) \times 510\ cm_{ECSA}^{2}} = 0.056\ H_2\ s^{-1}$$

Table S5. Summary of representative WP-based HER catalysts in 1 M KOH

Catalysts	η_{10} (mV)	Tafel slope (mV dec^{-1})	Loading (mg cm^{-2})	Journal
$Co_{0.9}W_{1.1}P_2/C$[2]	54	59	0.283	Nano Research (2021)
a-WNP[4]	70	39	1	J. Mater. Chem. A (2021)
W_2C/WP@NC-2[1]	116	59	1	ACS applied materials & interfaces (2021)
WP-Mesop[16]	149	66	2	ACS applied materials & interfaces (2020)
WP@NC[17]	232	88	0.285	ACS Appl. Energy Mater. (2020)
Co-WP[18]	119	55	0.2	Applied Catalysis B: Environmental (2019)
WP[18]	261	112	0.2	Applied Catalysis B: Environmental (2019)
S-CoWP@S,N-C[19]	61	61	0.75	ACS Energy Letters (2018)
W-SAC[9]	85	53	0.204	Advanced Materials (2018)
$Ni(OH)_2$ -WP/CP[20]	77	71	/	CHEMSUSCHEM (2018)
WP_2[21]	141	86	2	Journal of Power Sources (2017)
C-WP/W[12]	133	70	5	Chem. Eng. J, 327 (2017)
WP NAs[7]	150	102	2	ACS applied materials & interfaces (2014)
W_3P/WP/W	**146**	**58**	**0.1215**	**This work**

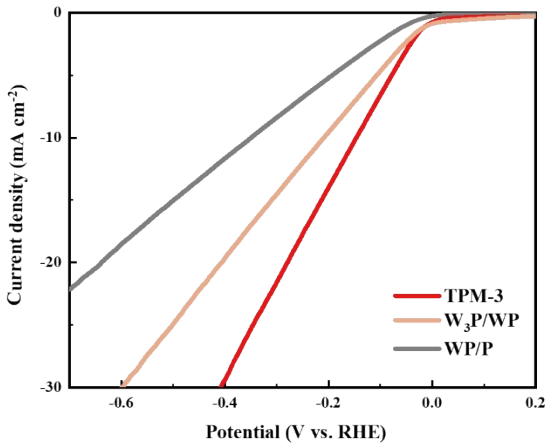

Figure S10. LSV curves of TMP-3, W_3P/WP, and WP/W in 1 M KOH.

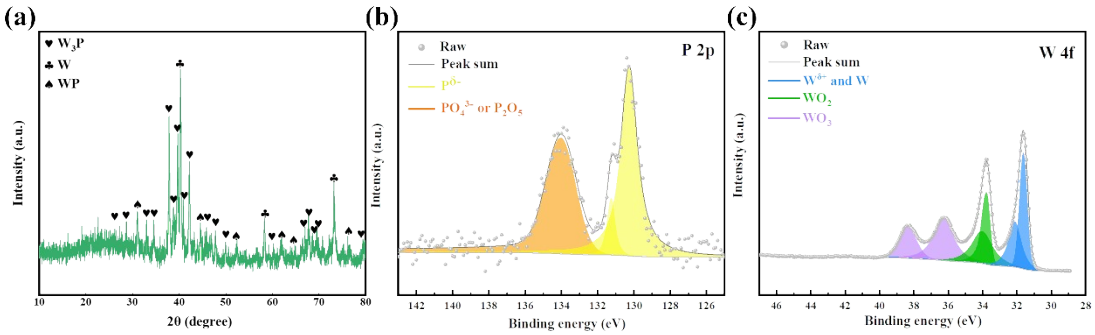

Figure S11. Characterizations of the catalyst after long-term stability test in 1 M KOH. (a) XRD pattern; (b) XPS P 2p; (c) XPS W 4f.

Table S6. Electrochemical impedance parameters obtained by fitting the Nyquist Plots to the equivalent circuit model (1 M KOH).

Catalyst	R_s (Ω)	R_p (Ω)	R_{ct} (Ω)
TPM-1	31.16	31.04	998.9
TPM-2	29.88	38.81	925.0
TPM-3	37.32	44.54	431.2
TPM-4	43.64	49.76	1156.4
W_3P/WP	59.66	198.75	1279.3
WP/W	58.77	67.59	1934.6

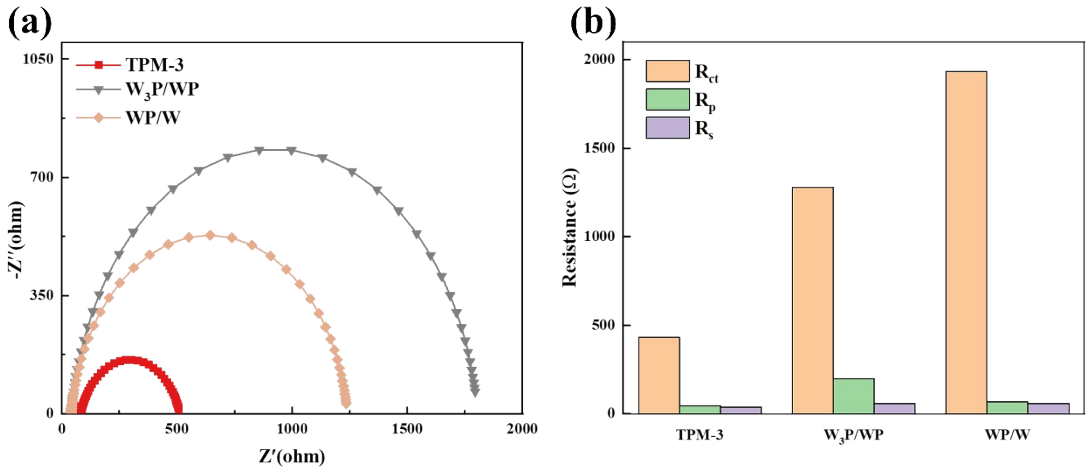

Figure S12. Fitted Nyquist plots of TPM-3, W_3P/WP, and WP/W (a), and their R_{ct}, R_p, and R_s in 1 M KOH (b).

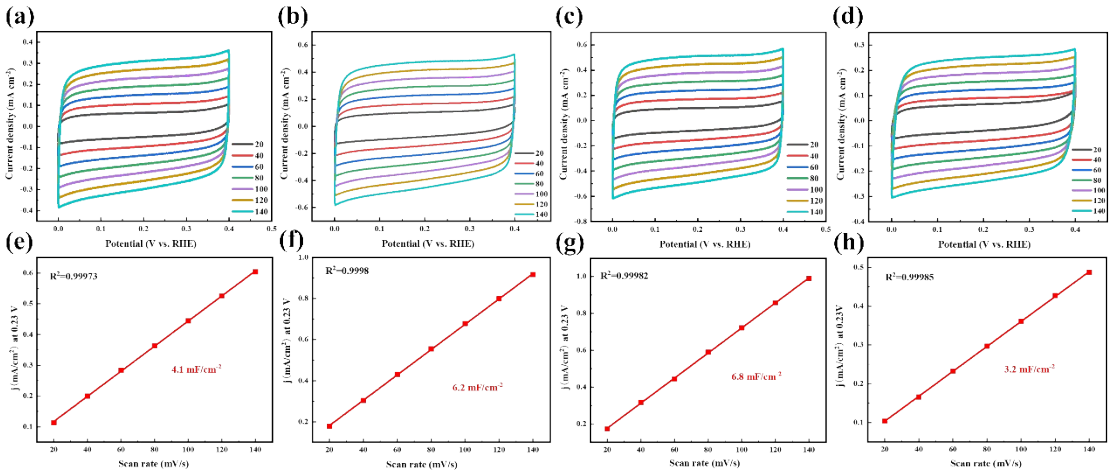

Figure S13. Cyclic voltammograms (a, b, c, d) and their corresponding plots (e, f, g, h) of the current density vs scan rate: TPM-1 (a, e), TPM-2 (b, f), TPM-3 (c, g), and TPM-4 (d, h) in 1 M KOH

Calculated Electrochemically Active Surface Area

For 1 M KOH,

TPM-1:

$$\text{ATPM-1 ECSA} = \frac{4.1/2 \text{ mF cm}^{-2}}{40 \text{ µF cm}^{-2} \text{ per cm}^2_{\text{ECSA}}} = 51.25 \text{ cm2 ECSA}$$

TPM-2:

$$\text{ATPM-2 ECSA} = \frac{6.2/2 \text{ mF cm}^{-2}}{40 \text{ µF cm}^{-2} \text{ per cm}^2_{\text{ECSA}}} = 77.5 \text{ cm2 ECSA}$$

TPM-3:

$$\text{ATPM-3 ECSA} = \frac{6.8/2 \text{ mF cm}^{-2}}{40 \text{ µF cm}^{-2} \text{ per cm}^2_{\text{ECSA}}} = 85.0 \text{ cm2 ECSA}$$

TPM-4:

$$\text{ATPM-4 ECSA} = \frac{3.2/2\ \text{mF cm}^{-2}}{40\ \mu\text{F cm}^{-2}\ \text{per cm}^2_{\text{ECSA}}} = 40.0\text{cm2 ECSA}$$

Calculated TOF values at an overpotential of -300 mV

The plot of current density can be converted into a TOF plot according to:

$$\text{TOF} = \frac{(3.12 \times 10^{15}\ \frac{\text{H}_2\ \text{s}^{-1}}{\text{cm}^2}\ \text{per}\ \frac{\text{mA}}{\text{cm}^2}) \times |\text{j}|}{(Active\ sites) \times\ \text{A}_{\text{ECSA}}}$$

TPM-1:

$$\text{TOF}_{\text{TPM-1}} = \frac{(3.12 \times 10^{15}\ \frac{\text{H}_2\ \text{s}^{-1}}{\text{cm}^2}\ \text{per}\ \frac{\text{mA}}{\text{cm}^2}) \times \left| -12.11\text{mA cm}^{-2} \right|}{\left(1.6809 \times 10^{15}\ \text{atoms cm}^{-2}_{\text{real}}\right) \times\ 51.25\ \text{cm}^2_{\text{ECSA}}} = 0.439\ \text{H}_2\ \text{s}^{-1}$$

TPM-2:

$$\text{TOF}_{\text{TPM-2}} = \frac{(3.12 \times 10^{15}\ \frac{\text{H}_2\ \text{s}^{-1}}{\text{cm}^2}\ \text{per}\ \frac{\text{mA}}{\text{cm}^2}) \times \left| -18.38\ \text{mA cm}^{-2} \right|}{\left(1.6796 \times 10^{15}\ \text{atoms cm}^{-2}_{\text{real}}\right) \times\ 77.5\ \text{cm}^2_{\text{ECSA}}} = 0.441\ \text{H}_2\ \text{s}^{-1}$$

TPM-3:

$$\text{TOF}_{\text{TPM-3}} = \frac{(3.12 \times 10^{15}\ \frac{\text{H}_2\ \text{s}^{-1}}{\text{cm}^2}\ \text{per}\ \frac{\text{mA}}{\text{cm}^2}) \times \left| -21.57\ \text{mA cm}^{-2} \right|}{\left(1.6755 \times 10^{15}\ \text{atoms cm}^{-2}_{\text{real}}\right) \times\ 85\ \text{cm}^2_{\text{ECSA}}} = 0.473\ \text{H}_2$$

s^{-1}

TPM-4:

$$\text{TOF}_{\text{TPM-4}} = \frac{\left(3.12 \times 10^{15} \frac{H_2\ s^{-1}}{cm^2}\ \text{per}\ \frac{mA}{cm^2}\right) \times \left| -10.57\ mA\ cm^{-2} \right|}{\left(1.6812 \times 10^{15}\ \text{atoms}\ cm_{real}^{-2}\right) \times 40\ cm_{ECSA}^{2}} = 0.490\ H_2\ s^{-1}$$

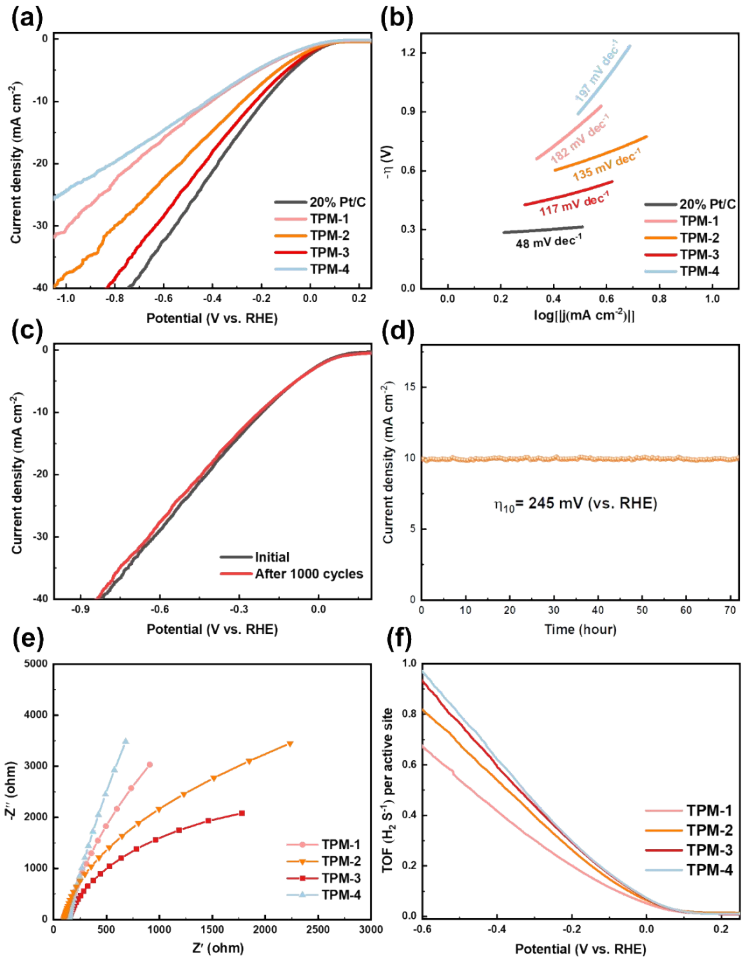

Figure S14. Electrocatalytic HER performance of TPM-1, TPM-2, TPM-3, TPM-4, as well as 20 wt % Pt/C in neutral (1 M PBS) media. (a) Polarization curves; (b) corresponding Tafel slope diagrams; (c) LSV curves before and after 1000 cycles for TPM-3; (d) i-t curve at overpotential of 245 mV for TPM-3; (e) EIS curves and (f) TOF profiles of TPMs.

Table S7. Summary of representative HER catalysts in 1 M PBS

Catalysts	η_{10} (mV)	Tafel slope (mV dec^{-1})	Loading (mg cm^{-2})	Journal
Ni/NBCF-2-H_2[22]	159	471	2.4	Journal of Colloid and Interface Science (2022)
$(Fe,Ni)_3P$/NiCoP[23]	70.5	112.9	5.3	Chemical Engineering Journal (2022)
MoS_2/α-MoC[24]	176	50.8	0.4	ACS Nano (2021)
La-MoP@NC[25]	235.27	141.13	2.0	Applied Catalysis B: Environmental (2021)
Cu-CoP NAs/CP[26]	81	83.5	5.17	Applied Catalysis B: Environmental (2020)
S-MoP NPL[27]	142	98	/	ACS Catalysis (2019)
MoP@NPC-H[28]	198	94	0.1989	ACS Sustainable Chemistry & Engineering (2018)
Co_9S_8/NC@MoS_2[29]	261	126.1	0.283	ACS Appl. Mater. Interfaces (2017)
CoP@BCN[30]	122	59	0.4	Adv. Energy Mater (2016)
WP_2 NPs/W[31]	201	95	0.2	Energy Technology (2016)
WP NPs@NC[13]	196	58	2.0	J. Mater. Chem. A (2016)
MoP NPs[32]	330	50	0.1	J. Mater. Chem. A (2015)

np-CoP NWs/Ti[33]	178	125	0.8	Phys. Chem. Chem. Phys (2014)
WP NAs/CC[7]	200	125	2.0	ACS Appl. Mater. Interfaces (2014)
W_3P/WP/W	**245**	**117**	**0.1215**	**This work**

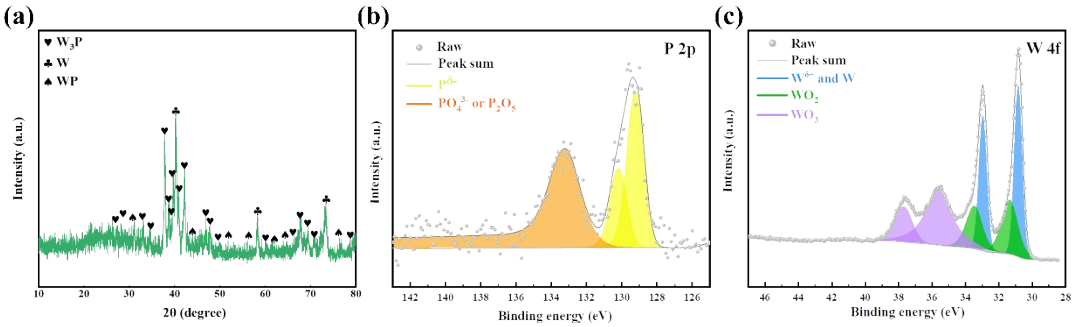

Figure S15. Characterizations of the catalyst after long-term stability test in 1 M PBS. (a) XRD pattern; (b) XPS P 2p; (c) XPS W 4f.

Table S8. Electrochemical impedance parameters obtained by fitting the Nyquist Plots to the equivalent circuit model (1 M PBS).

Catalyst	**R_s (Ω)**	**R_p (Ω)**	**R_{ct} (Ω)**
TPM-1	129.3	16.16	5236

TPM-2	133.5	14.87	4377
TPM-3	104.2	15.7	3065
TPM-4	125.9	16.07	8581

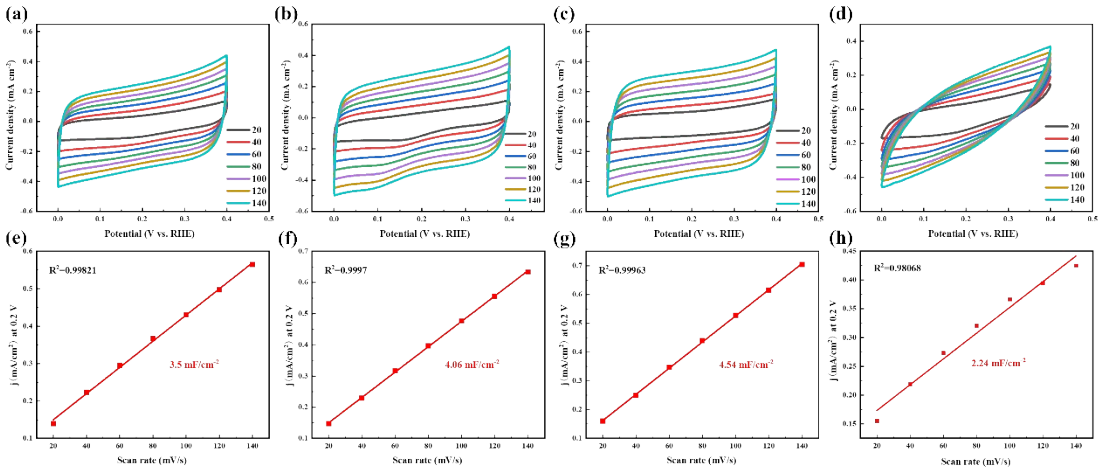

Figure S16. Cyclic voltammograms (a, b, c, d) and their corresponding plots (e, f, g, h) of the current density vs scan rate: TPM-1 (a, e), TPM-2 (b, f), TPM-3 (c, g), and TPM-4 (d, h) in 1 M PBS.

Calculated Electrochemically Active Surface Area

For 1 M PBS,

TPM-1:

$$\text{ATPM-1 ECSA} = \frac{3.5/2 \text{ mF cm}^{-2}}{40 \text{ µF cm}^{-2} \text{ per cm}^2_{\text{ECSA}}} = 43.75 \text{ cm2 ECSA}$$

TPM-2:

$$\text{ATPM-2 ECSA} = \frac{4.06/2 \text{ mF cm}^{-2}}{40 \text{ µF cm}^{-2} \text{ per cm}^2_{\text{ECSA}}} = 50.75 \text{ cm2 ECSA}$$

TPM-3:

$$\text{ATPM-3 ECSA} = \frac{4.54/2 \text{ mF cm}^{-2}}{40 \text{ } \mu\text{F cm}^{-2} \text{ per cm}^2_{\text{ECSA}}} = 56.75 \text{ cm2 ECSA}$$

TPM-4:

$$\text{ATPM-4 ECSA} = \frac{2.24/2 \text{ mF cm}^{-2}}{40 \text{ } \mu\text{F cm}^{-2} \text{ per cm}^2_{\text{ECSA}}} = 28.0 \text{ cm2 ECSA}$$

Calculated TOF values at an overpotential of -300 mV

The plot of current density can be converted into a TOF plot according to:

$$\text{TOF} = \frac{(3.12 \times 10^{15} \frac{\text{H}_2 \text{ s}^{-1}}{\text{cm}^2} \text{ per } \frac{\text{mA}}{\text{cm}^2}) \times |\text{j}|}{(Active\ sites) \times \text{A}_{\text{ECSA}}}$$

TPM-1:

$$\text{TOF}_{\text{TPM-1}} = \frac{(3.12 \times 10^{15} \frac{\text{H}_2 \text{ s}^{-1}}{\text{cm}^2} \text{ per } \frac{\text{mA}}{\text{cm}^2}) \times \left| -7.13 \text{mA cm}^{-2} \right|}{\left(1.6809 \times 10^{15} \text{ atoms cm}^{-2}_{\text{real}}\right) \times 43.75 \text{ cm}^2_{\text{ECSA}}} = 0.302 \text{ H}_2 \text{ s}^{-1}$$

TPM-2:

$$\text{TOF}_{\text{TPM-2}} = \frac{(3.12 \times 10^{15} \frac{\text{H}_2 \text{ s}^{-1}}{\text{cm}^2} \text{ per } \frac{\text{mA}}{\text{cm}^2}) \times \left| -10.89 \text{ mA cm}^{-2} \right|}{\left(1.6796 \times 10^{15} \text{ atoms cm}^{-2}_{\text{real}}\right) \times 50.75 \text{ cm}^2_{\text{ECSA}}} = 0.399 \text{ H}_2 \text{ s}^{-1}$$

TPM-3:

$$TOF_{TPM\text{-}3} = \frac{(3.12 \times 10^{15} \frac{H_2\ s^{-1}}{cm^2}\ per\ \frac{mA}{cm^2}) \times \left| -13.36\ mA\ cm^{-2} \right|}{\left(1.6755 \times 10^{15}\ atoms\ cm_{real}^{-2}\right) \times 56.75\ cm_{ECSA}^{2}} = 0.438\ H_2\ s^{-1}$$

TPM-4:

$$TOF_{TPM\text{-}4} = \frac{(3.12 \times 10^{15} \frac{H_2\ s^{-1}}{cm^2}\ per\ \frac{mA}{cm^2}) \times \left| -6.84\ mA\ cm^{-2} \right|}{\left(1.6812 \times 10^{15}\ atoms\ cm_{real}^{-2}\right) \times 28\ cm_{ECSA}^{2}} = 0.453\ H_2\ s^{-1}$$

Table S9. Summary of representative HER catalysts in simulated/natural/treated natural seawater

Catalysts	Electrolyte	η_{10}	η_{100}	Stability	Loading (mg cm^{-2})	Journal
C-Co$_2$P[34]	Artificial alkaline seawater	1.55 V	1.68 V	10-1000 mA cm^{-2} @60 h	2.18	Advanced Functional Materials (2021)
Ni$_2$P-Fe$_2$P[35]	1 M KOH+ seawater	/	1.811 V	100 mA cm^{-2} @48 h	15.0	Advanced Functional Materials (2021)
Fe-MoS$_2$ NSA[36]	Buffered seawater	119 mV (overpotential)	300 mV (overpotential)	100 mA cm^{-2} @30 h	0.5	Nanotechnology (2021)

S,P-(Ni,Mo,Fe)OOH/NiMoP /wood aerogel[37]	1 M KOH+ seawater	/	1.741 V	100/500 mA cm^{-2} @20/10 h	1	Applied Catalysis B: Environmental (2021)
Cu_2S@Ni[38]	1 M NaOH+ 0.5 M NaCl	/	1.78 V	100/200/400 mA cm^{-2} @50 h	/	Journal of Power Sources (2021)
Fe-Co_2P BNR[39]	Seawater	489 mV (overpotential)	780 mV (overpotential) for 350 mA cm^{-2}	200 mA cm^{-2} @48 h	1	Journal of Energy Chemistry (2021)
NiCoFeP/Ni foam[40]	6 M KOH+ 0.5 M NaCl	/	1.64 V	500 mA cm^{-2} @100 h	2	RESEARCH (2020)
GO@Fe@NiCo@NF[41]	1 M KOH + 0.5 M NaCl	1.57 V (20 mA cm^{-2})	/	1000 mA cm^{-2} @378 h	1.9	Journal of Materials Chemistry A (2020)
NiNS (Ni_3N and Ni_3S_2)[42]	Seawater	1.8 V (48.3 mA cm^{-2})	/	1.88 V @12 h	19.95	Journal of Materials Chemistry A (2019)
NiMoN nanorod[43]	1 M KOH + seawater	/	1.581 V	500 mA cm^{-2} @100 h	40	NATURE COMMUNICATIONS (2019)
Co–Se4[44]	Seawater	1.8 V	/	1.95 V @12 h	18.4	ADVANCED ENERGY MATERIALS (2018)
W_3P/WP/W	Artificial alkaline seawater	**1.165 V**	/	10 mA cm^{-2} @72 h	**0.1215**	**This work**
	Seawater	**0.998 V**	**2.255 V**	100 mA cm^{-2} @72 h	**0.1215**	
	1 M KOH + seawater	**0.966 V**	**1.441 V**	100 mA cm^{-2} @ 72 h	**0.1215**	
	Ion exchange resins purified seawater	**0.917 V**	**1.729 V**	100 mA cm^{-2} @ 200 h	**0.1215**	

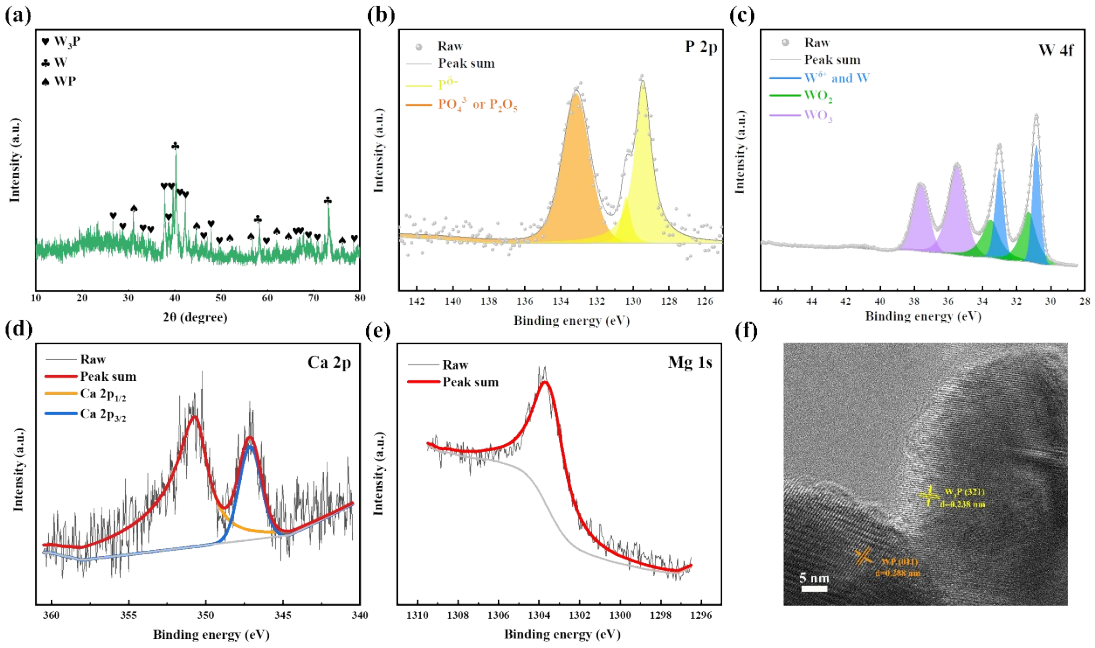

Figure S17. Characterizations of TPM-3 after long-term stability test in simulated seawater. (a) XRD pattern; (b) XPS P 2p; (c) XPS W 4f; (d) XPS Ca 2p; (e) XPS Mg 1s, and (e) TEM

Table S10. The concentration of element Ca, Mg before and after the stability test in four different electrolytes (Pt/C and TPM-3).

Electrolyte	Mg (mg/L) Before reaction	Mg (mg/L) After reaction		Ca (mg/L) Before rection	Ca (mg/L) After reaction	
		TPM-3	Pt/C		TPM-3	Pt/C
Artificial alkaline seawater	954	903	913	490	468	462
Seawater	4860	3076	2358	1350	964	720
1 M KOH + seawater	140	127	121	538	513	497
Ion exchange resins purified seawater	374	350	294	213	208	199

Figure S18. The natural seawater obtained from Xinghai Bay in Dalian, Liaoning, China. The bottle has been washed with deionized water more than 10 times.

Table S11. Date and geographical parameters of the collection location

Item	Parameter
Date	2022-01-06 12:56 pm
Longitude	121.5644 'E
Latitude	38.8759 'N
Altitude	3 m
Body temperature	-4 °C
Humidity	41%
Atmospheric pressure	1.034×10^5 Pa

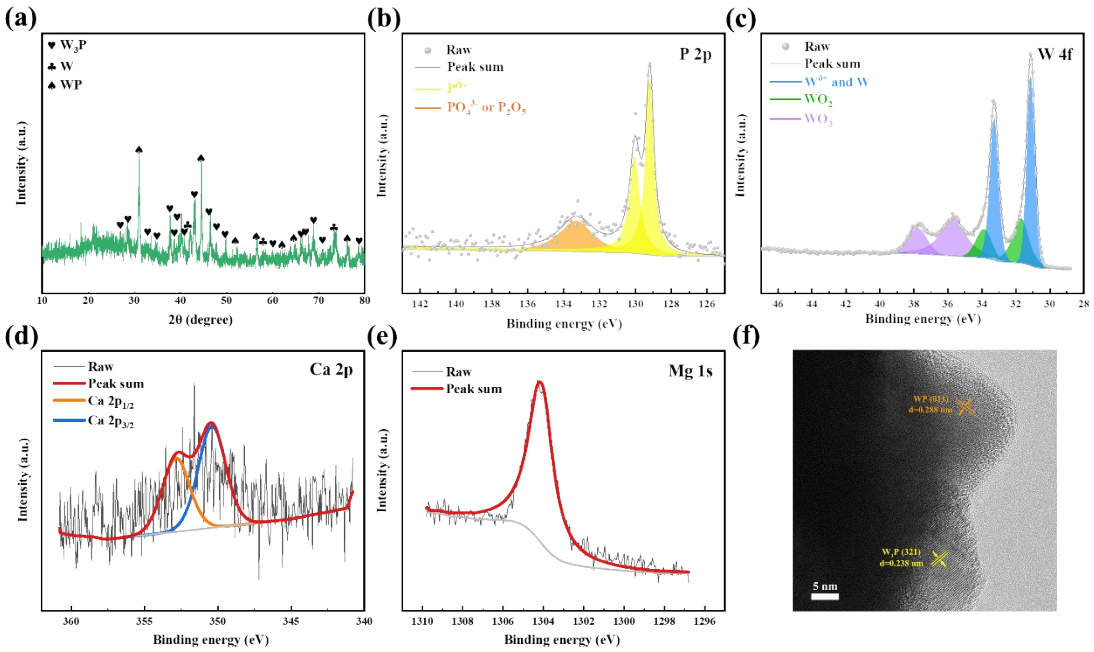

Figure S19. Characterizations of TPM-3 after long-term stability test in natural seawater. (a) XRD pattern; (b) XPS P 2p; (c) XPS W 4f; (d) XPS Ca 2p; (e) XPS Mg 1s, and (e) TEM

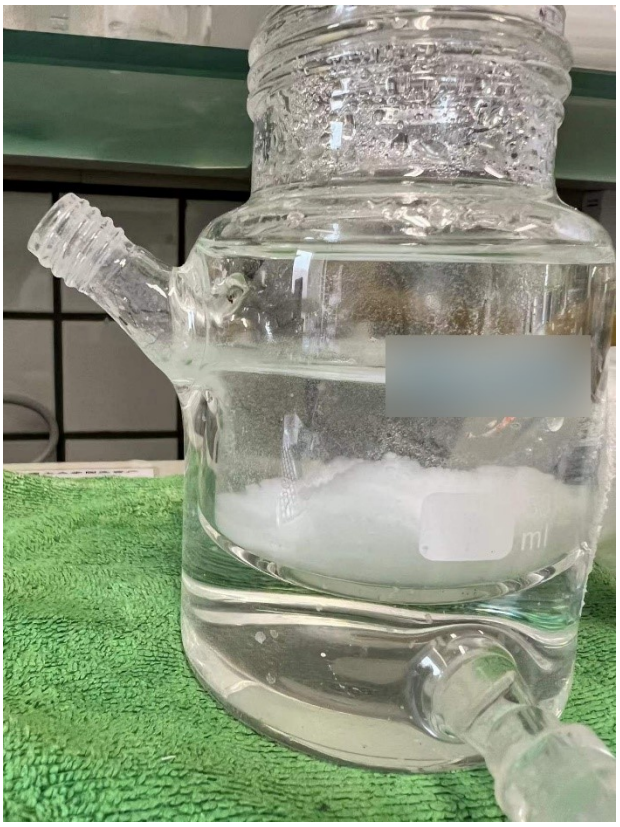

Figure S20. After 72 hours' long term operation, plenty of white flocculent precipitates, $Ca(OH)_2$ and $Mg(OH)_2$, appeared at the bottom of the electrolytic cell.

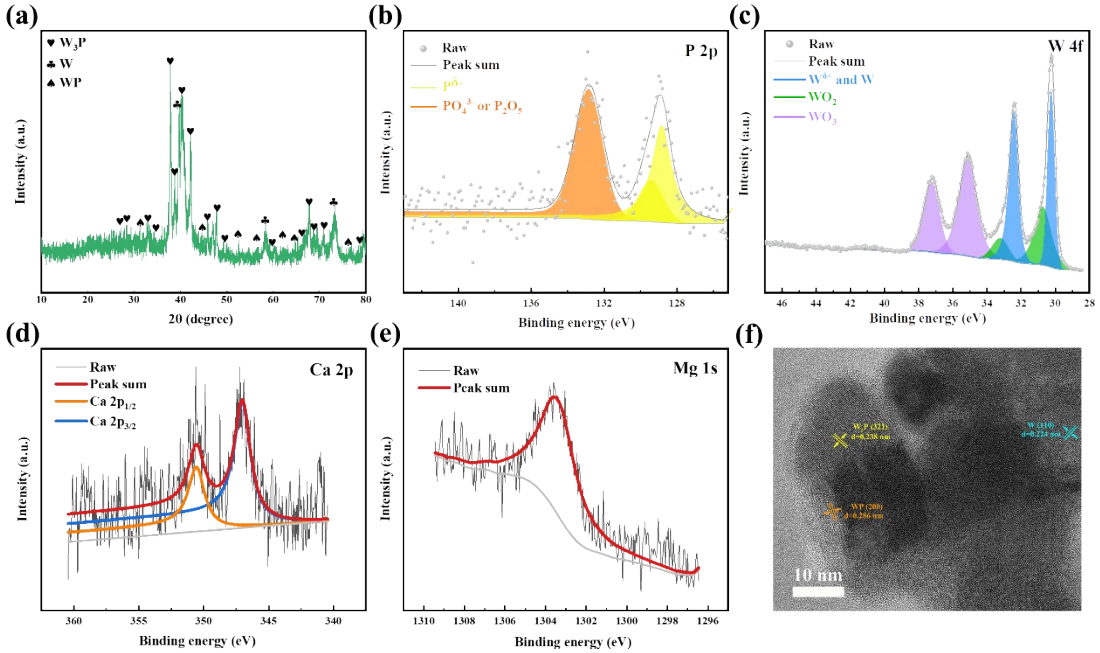

Figure S21. Characterizations of TPM-3 after long-term stability test in 1 M KOH+ seawater. (a) XRD pattern; (b) XPS P 2p; (c) XPS W 4f; (d) XPS Ca 2p; (e) XPS Mg 1s, and (e) TEM.

Pretreatment of ion exchange resin:

Place the resin in a clean container and rinse with water until the drainage is clear. Soak the resin with water for 24 hours to fully swell the resin. The resin was then soaked in 5% HCl solution (twice the volume of the resin) for 4 hours with constant stirring. Then wash the resin with ultrapure water until the pH of the solution is close to 4, then treat with 2~5% NaOH solution, and wash with ultrapure water until neutral.

Regeneration of ion exchange resin:

Rinse the resin with clean water and filter dry. Then soak in 80%~90% ethanol for 24 hours to wash away the ethanol-soluble organic matter in the resin. Soak in hot water at 40 ℃ for 2 hours and wash several times to remove water-soluble impurities. Then drain. Soak for 2 hours with a hydrochloric acid solution (2 mol/L, 4 times the amount of resin) to wash away acid-soluble impurities. Wash until neutral and drain. Soak in sodium chloride (2 mol/L, 4 times the amount of resin) solution for 2 hours, then wash until neutral, drain and set aside.

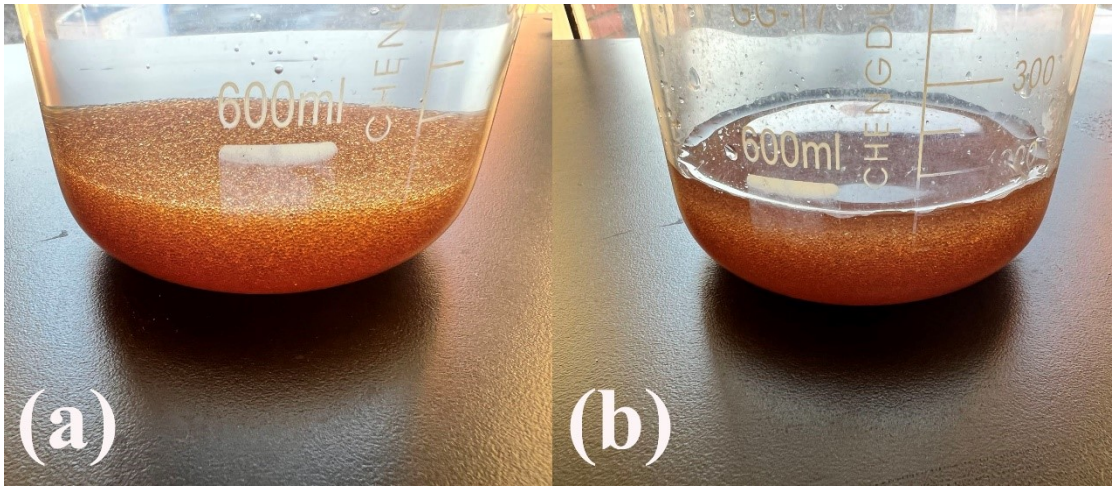

Figure S22. Ion exchange resins before (a) and after (b) been used to remove calcium and magnesium ions in natural seawater.

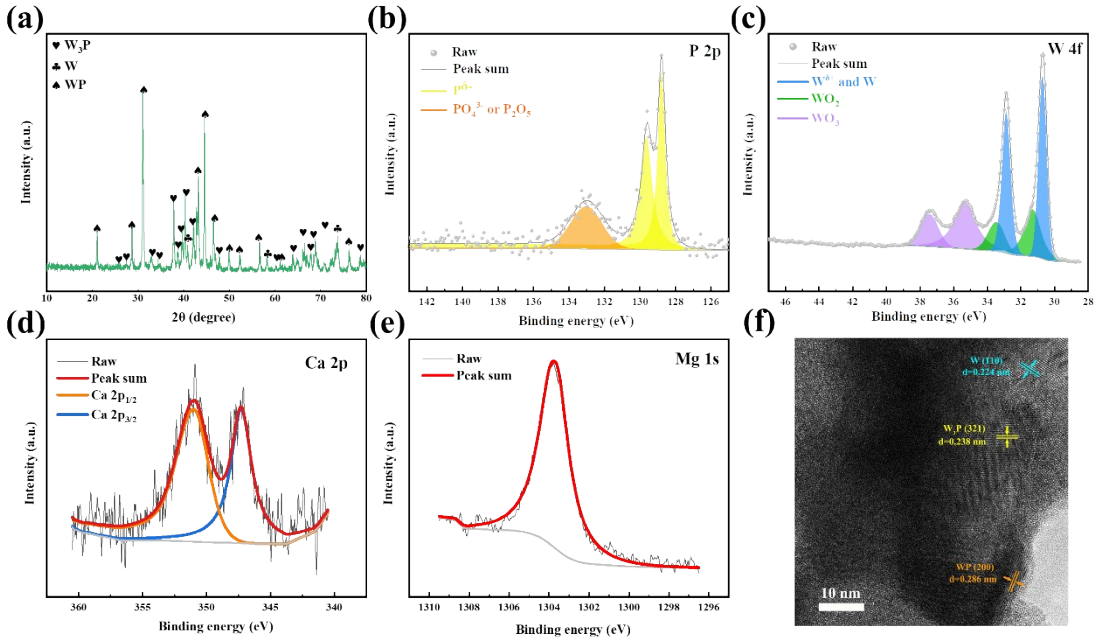

Figure S23. Characterizations of TPM-3 after long-term stability test in Ion exchange resins purified seawater. (a) XRD pattern; (b) XPS P 2p; (c) XPS W 4f; (d) XPS Ca 2p; (e) XPS Mg 1s, and (e) TEM.

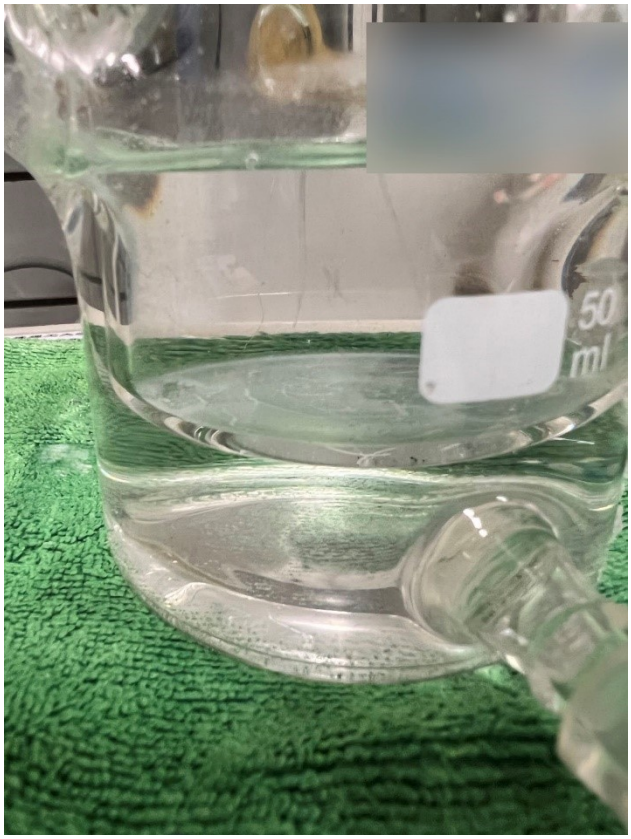

Figure S24. Almost no precipitation in the electrolytic cell after 200 hours of stability test

References

1 Wei, P.; Sun, X.; Wang, M.; Xu, J.; He, Z.; Li, X.; Cheng, F.; Xu, Y.; Li, Q.; Han, J.; Yang, H.; Huang, Y., Construction of an N-Decorated Carbon-Encapsulated W_2C/WP Heterostructure as an Efficient Electrocatalyst for Hydrogen Evolution in Both Alkaline and Acidic Media. *ACS Appl Mater Interfaces.* **2021,** *13* (45), 53955-53964.

2 Zhang, B.; Li, C.; Hu, J.; Peng, D.; Huang, K.; Wu, J.; Chen, Z.; Huang, Y., Cobalt tungsten phosphide with tunable W-doping as highly efficient electrocatalysts for hydrogen evolution reaction. *Nano Research.* **2021,** *14* (11), 4073-4078.

3 Huo, D.; Sun, Z.; Liu, Y.; Yu, Z.; Wang, Y.; Wang, A., Synthesis of Co-Doped Tungsten Phosphide Nanoparticles Supported on Carbon Supports as High-Efficiency HER Catalysts. *ACS Sustainable Chemistry & Engineering.* **2021,** *9* (36), 12311-12322.

4 Jin, Z. Y.; Li, P. P.; Huang, X.; Zeng, G. F.; Jin, Y.; Zheng, B. Z.; Xiao, D., Three-dimensional amorphous tungsten-doped nickel phosphide microsphere as an efficient electrocatalyst for hydrogen evolution. *Journal of Materials Chemistry A.* **2014,** *2* (43), 18593-18599.

5 Liu, W.; Geng, P.; Li, S.; Zhu, R.; Liu, W.; Lu, H.; Chandrasekaran, S.; Pang, Y.; Fan, D.; Liu, Y., Self-supported three-dimensional WP_2 (WP) nanosheet arrays for efficient electrocatalytic hydrogen evolution. *Int. J. Hydrogen Energy.* **2020,** *45* (53), 28576-28585.

6 Li, F.; Wang, C.; Han, X.; Feng, X.; Qu, Y.; Liu, J.; Chen, W.; Zhao, L.; Song, X.; Zhu, H.; Chen, H.; Zhao, M.; Deng, Z.; Wu, J.; Zhang, P.; Gao, L., Confinement Effect of Mesopores: In Situ Synthesis of Cationic Tungsten-Vacancies for a Highly Ordered Mesoporous Tungsten Phosphide Electrocatalyst. *ACS Applied Materials & Interfaces.* **2020,** *12* (20), 22741-22750.

7 Pu, Z.; Liu, Q.; Asiri, A. M.; Sun, X., Tungsten Phosphide Nanorod Arrays Directly Grown on Carbon Cloth: A Highly Efficient and Stable Hydrogen Evolution Cathode at All pH Values. *Acs Applied Materials & Interfaces.* **2014,** *6* (24), 21874-21879.

8 Wang, J.; Chang, K.; Sun, Z.; Lee, J. H.; Tackett, B. M.; Zhang, C.; Chen, J. G.; Liu, C.-J., A Combined experimental and theoretical study of the accelerated hydrogen evolution kinetics over wide pH range on porous transition metal doped tungsten phosphide electrocatalysts. *Appl. Catal. B-Environ.* **2019,** *251*, 162-167.

9 Chen, W. X.; Pei, J. J.; He, C. T.; Wan, J. W.; Ren, H. L.; Wang, Y.; Dong, J. C.; Wu, K. L.; Cheong, W. C.; Mao, J. J.; Zheng, X. S.; Yan, W. S.; Zhuang, Z. B.; Chen, C.; Peng, Q.; Wang, D. S.; Li, Y. D., Single Tungsten Atoms Supported on MOF-Derived N-Doped Carbon for Robust Electrochemical Hydrogen Evolution. *Adv. Mater.* **2018,** *30* (30), 6.

10. Xu, K.; Fu, X.; Li, H.; Peng, Z., A novel composite of network-like tungsten phosphide nanostructures grown on carbon fibers with enhanced electrocatalytic hydrogen evolution efficiency. *Appl. Surf. Sci.* **2018,** *456*, 230-237.

11 Shi, M.; Li, W.; Fang, J.; Jiang, Z.; Gao, J.; Chen, Z.; Sun, F.; Xu, Y., Electronic structure tuning during facile construction of two-phase tungsten based electrocatalyst for hydrogen evolution reaction. *Electrochim. Acta* **2018,** *283*, 834-841.
12 Wu, L.; Pu, Z.; Tu, Z.; Amiinu, I. S.; Liu, S.; Wang, P.; Mu, S., Integrated design and construction of WP/W nanorod array electrodes toward efficient hydrogen evolution reaction. *Chem. Eng. J.* **2017,** *327*, 705-712.
13 Pu, Z.; Ya, X.; Amiinu, I. S.; Tu, Z.; Liu, X.; Li, W.; Mu, S., Ultrasmall tungsten phosphide nanoparticles embedded in nitrogen-doped carbon as a highly active and stable hydrogen-evolution electrocatalyst. *Journal of Materials Chemistry A.* **2016,** *4* (40), 15327-15332.
14 Yang, L.; Xu, P.; Zhang, W.; Chen, M.; Feng, C.; Yuan, X., Facile synthesis of one-dimensional MoWP hybrid nanowires and their enhanced electrochemical catalytic activities. *Chem. Phys. Lett.* **2020,** *741*.
15 Adam, A.; Suliman, M. H.; Dafalla, H.; Al-Arfaj, A. R.; Siddiqui, M. N.; Qamar, M., Rationally Dispersed Molybdenum Phosphide on Carbon Nanotubes for the Hydrogen Evolution Reaction. *ACS Sustainable Chemistry & Engineering.***2018,** *6* (9), 11414-11423.
16 Li, F.; Wang, C.; Han, X.; Feng, X.; Qu, Y.; Liu, J.; Chen, W.; Zhao, L.; Song, X.; Zhu, H.; Chen, H.; Zhao, M.; Deng, Z.; Wu, J.; Zhang, P.; Gao, L., Confinement Effect of Mesopores: In Situ Synthesis of Cationic Tungsten-Vacancies for a Highly Ordered Mesoporous Tungsten Phosphide Electrocatalyst. *ACS Appl Mater Interfaces.* **2020,** *12* (20), 22741-22750.
17 Chakrabartty, S.; Sahu, D.; Raj, C. R., General Approach for the Synthesis of Nitrogen-Doped Carbon Encapsulated Mo and W Phosphide Nanostructures for Electrocatalytic Hydrogen Evolution. *ACS Applied Energy Materials.* **2020,** *3* (3), 2811-2820.
18 Wang, J.; Chang, K.; Sun, Z.; Lee, J. H.; Tackett, B. M.; Zhang, C.; Chen, J. G.; Liu, C.-J., A Combined experimental and theoretical study of the accelerated hydrogen evolution kinetics over wide pH range on porous transition metal doped tungsten phosphide electrocatalysts. *Applied Catalysis B: Environmental.* **2019,** *251*, 162-167.
19 Weng, B. C.; Grice, C. R.; Meng, W. W.; Guan, L.; Xu, F. H.; Yu, Y.; Wang, C. L.; Zhao, D. W.; Yan, Y. F., Metal-Organic Framework-Derived CoWP@C Composite Nanowire Electrocatalyst for Efficient Water Splitting. *ACS Energy Lett.* **2018,** *3* (6), 1434-1442.
20 Kim, D.; Park, J.; Lee, J.; Zhang, Z.; Yong, K. J., $Ni(OH)_2$-WP Hybrid Nanorod Arrays for Highly Efficient and Durable Hydrogen Evolution Reactions in Alkaline Media. *Chemsuschem.* **2018,** *11* (20), 3618-3624.
21 Pi, M. Y.; Wu, T. L.; Guo, W. M.; Wang, X. D.; Zhang, D. K.; Wang, S. X.; Chen, S. J., Phase-controlled synthesis of polymorphic tungsten diphosphide with hybridization of monoclinic and orthorhombic phases as a novel electrocatalyst for efficient hydrogen evolution. *J. Power Sources.* **2017,** *349*, 138-143.
22 Hong, S.; Song, N.; Jiang, E.; Sun, J.; Chen, G.; Li, C.; Liu, Y.; Dong, H., Nickel supported on Nitrogen-doped biomass carbon fiber fabricated via in-situ template

technology for pH-universal electrocatalytic hydrogen evolution. *J. Colloid Interface Sci.* **2022,** *608* (Pt 2), 1441-1448.
23 Li, W.; Cheng, G.; Peng, S.; Sun, M.; Wang, S.; Han, S.; Liu, Y.; Zhai, T.; Yu, L., Tuning hydrogen binding energy by interfacial charge transfer enables pH-universal hydrogen evolution catalysis of metal phosphides. *Chem. Eng. J.* **2022,** *430*.
24 Cheng, Z.; Xiao, Y.; Wu, W.; Zhang, X.; Fu, Q.; Zhao, Y.; Qu, L., All-pH-Tolerant In-Plane Heterostructures for Efficient Hydrogen Evolution Reaction. *ACS Nano* **2021**.
25 Wei, P.; Li, X.; He, Z.; Li, Z.; Zhang, X.; Sun, X.; Li, Q.; Yang, H.; Han, J.; Huang, Y., Electron density modulation of MoP by rare earth metal as highly efficient electrocatalysts for pH-universal hydrogen evolution reaction. *Applied Catalysis B: Environmental* **2021,** *299*.
26 Yan, L.; Zhang, B.; Zhu, J.; Li, Y.; Tsiakaras, P.; Kang Shen, P., Electronic modulation of cobalt phosphide nanosheet arrays via copper doping for highly efficient neutral-pH overall water splitting. *Applied Catalysis B: Environmental.* **2020,** *265*.
27 Liang, K.; Pakhira, S.; Yang, Z.; Nijamudheen, A.; Ju, L.; Wang, M.; Aguirre-Velez, C. I.; Sterbinsky, G. E.; Du, Y.; Feng, Z.; Mendoza-Cortes, J. L.; Yang, Y., S-Doped MoP Nanoporous Layer Toward High-Efficiency Hydrogen Evolution in pH-Universal Electrolyte. *ACS Catalysis.* **2018,** *9* (1), 651-659.
28 Chi, J.-Q.; Gao, W.-K.; Zhang, L.-M.; Dong, B.; Yan, K.-L.; Lin, J.-H.; Liu, B.; Chai, Y.-M.; Liu, C.-G., Induced Phosphorization-Derived Well-Dispersed Molybdenum Phosphide Nanoparticles Encapsulated in Hollow N-Doped Carbon Nanospheres for Efficient Hydrogen Evolution. *ACS Sustainable Chemistry & Engineering.* **2018,** *6* (6), 7676-7686.
29 Li, H.; Qian, X.; Xu, C.; Huang, S.; Zhu, C.; Jiang, X.; Shao, L.; Hou, L., Hierarchical Porous Co_9S_8/Nitrogen-Doped Carbon@MoS_2 Polyhedrons as pH Universal Electrocatalysts for Highly Efficient Hydrogen Evolution Reaction. *ACS Appl Mater Interfaces.* **2017,** *9* (34), 28394-28405.
30 Tabassum, H.; Guo, W.; Meng, W.; Mahmood, A.; Zhao, R.; Wang, Q.; Zou, R., Metal-Organic Frameworks Derived Cobalt Phosphide Architecture Encapsulated into B/N Co-Doped Graphene Nanotubes for All pH Value Electrochemical Hydrogen Evolution. *Advanced Energy Materials* **2017,** *7* (9).
31 Pu, Z.; Amiinu, I. S.; Mu, S., In Situ Fabrication of Tungsten Diphosphide Nanoparticles on Tungsten foil: A Hydrogen‐Evolution Cathode for a Wide pH Range. *Energy Technology.* **2016,** *4* (9), 1030-1034.
32 Wang, T. Y.; Du, K. Z.; Liu, W. L.; Zhu, Z. W.; Shao, Y. H.; Li, M. X., Enhanced electrocatalytic activity of MoP microparticles for hydrogen evolution by grinding and electrochemical activation. *Journal of Materials Chemistry A.* **2015,** *3* (8), 4368-4373.
33 Gu, S.; Du, H.; Asiri, A. M.; Sun, X.; Li, C. M., Three-dimensional interconnected network of nanoporous CoP nanowires as an efficient hydrogen evolution cathode. *Phys. Chem. Chem. Phys.* **2014,** *16* (32), 16909-13.

34 Xu, W.; Fan, G.; Zhu, S.; Liang, Y.; Cui, Z.; Li, Z.; Jiang, H.; Wu, S.; Cheng, F., Electronic Structure Modulation of Nanoporous Cobalt Phosphide by Carbon Doping for Alkaline Hydrogen Evolution Reaction. *Adv. Funct. Mater.* **2021,** *31* (48).
35 Wu, L.; Yu, L.; Zhang, F.; McElhenny, B.; Luo, D.; Karim, A.; Chen, S.; Ren, Z., Heterogeneous Bimetallic Phosphide Ni_2P-Fe_2P as an Efficient Bifunctional Catalyst for Water/Seawater Splitting. *Adv. Funct. Mater.* **2020,** *31* (1).
36 Huang, W.; Zhou, D.; Qi, G.; Liu, X., Fe-doped MoS_2 nanosheets array for high-current-density seawater electrolysis. *Nanotechnology.* **2021,** *32* (41).
37 Chen, H.; Zou, Y.; Li, J.; Zhang, K.; Xia, Y.; Hui, B.; Yang, D., Wood aerogel-derived sandwich-like layered nanoelectrodes for alkaline overall seawater electrosplitting. *Applied Catalysis B: Environmental.* **2021,** *293*.
38 Zhang, B.; Xu, W.; Liu, S.; Chen, X.; Ma, T.; Wang, G.; Lu, Z.; Sun, J., Enhanced interface interaction in Cu2S@Ni core-shell nanorod arrays as hydrogen evolution reaction electrode for alkaline seawater electrolysis. *J. Power Sources.* **2021,** *506*.
39 Lin, Y.; Sun, K.; Chen, X.; Chen, C.; Pan, Y.; Li, X.; Zhang, J., High-precision regulation synthesis of Fe-doped Co_2P nanorod bundles as efficient electrocatalysts for hydrogen evolution in all-pH range and seawater. *Journal of Energy Chemistry.* **2021,** *55*, 92-101.
40 Li, P. S.; Wang, S. Y.; Samo, I. A.; Zhang, X. H.; Wang, Z. L.; Wang, C.; Li, Y.; Du, Y. Y.; Zhong, Y.; Cheng, C. T.; Xu, W. W.; Liu, X. J.; Kuang, Y.; Lu, Z. Y.; Sun, X. M., Common-Ion Effect Triggered Highly Sustained Seawater Electrolysis with Additional NaCl Production. *Research.* **2020,** *2020*, 9.
41 Jadhav, A. R.; Kumar, A.; Lee, J.; Yang, T.; Na, S.; Lee, J.; Luo, Y.; Liu, X.; Hwang, Y.; Liu, Y.; Lee, H., Stable complete seawater electrolysis by using interfacial chloride ion blocking layer on catalyst surface. *Journal of Materials Chemistry A.* **2020,** *8* (46), 24501-24514.
42 Zhao, Y. Q.; Jin, B.; Vasileff, A.; Jiao, Y.; Qiao, S. Z., Interfacial nickel nitride/sulfide as a bifunctional electrode for highly efficient overall water/seawater electrolysis. *Journal of Materials Chemistry A.* **2019,** *7* (14), 8117-8121.
43 Yu, L.; Zhu, Q.; Song, S.; McElhenny, B.; Wang, D.; Wu, C.; Qin, Z.; Bao, J.; Yu, Y.; Chen, S.; Ren, Z., Non-noble metal-nitride based electrocatalysts for high-performance alkaline seawater electrolysis. *Nat Commun.* **2019,** *10* (1), 5106.
44 Zhao, Y.; Jin, B.; Zheng, Y.; Jin, H.; Jiao, Y.; Qiao, S. Z., Charge State Manipulation of Cobalt Selenide Catalyst for Overall Seawater Electrolysis. *Advanced Energy Materials.* **2018,** *8* (29).